

# INHIBITORY POTENTIAL OF BLACK SEED (*NIGELLA SATIVA* L.) BIOACTIVE COMPOUNDS TOWARDS MAIN PROTEASE OF SARS-CoV-2 : *IN SILICO* STUDY

Pamungkas Rizki Ferdian<sup>1\*</sup>, Rizki Rabeca Elfirta<sup>1</sup>, Qori Emilia<sup>1</sup>, Azra Zahrah Nadhirah Ikhwan<sup>1</sup>

<sup>1</sup>Research Center for Biology, Indonesian Institute of Sciences (LIPI), Jl. Raya Bogor Km.46, Cibinong, Bogor, 16911, Indonesia

## Abstract

COVID-19, caused by SARS-CoV-2, has become a massive worldwide concern of the 21<sup>st</sup> century. One potential strategy to block the biochemical pathway of SARS-CoV-2 was by inhibiting the main protease (Mpro), which is a key enzyme on viral replication. Black seed (*Nigella sativa* L.) has a long history for its use as a traditional medicine. Therefore, we hypothesised that the black seed contains numerous active compounds that could potentially confer inhibitory activity against SARS-CoV-2 viral Mpro. In this study, 24 active compounds from black seed were tested. Compounds were screened using Lipinski's Rules and admetSAR, then docked to viral Mpro 7BQY by AutoDockTools-1.5.6 and AutoDock Vina using a site directed docking approach resulting in affinity energy ( $\Delta G$ ) and binding data. We found that the most potential active compound of *N. sativa* is 3-[(4-Methylphenyl)sulfanyl]-1,3-diphenyl-1-propanone, since its affinity energy was  $-7.6 \text{ kCal.mol}^{-1}$ . Its similarity to N3 inhibitor based on Ligplot analysis and DS were 86.7% and 76.19%, respectively, and the occupancy on binding site based on Ligplot analysis and DS were 90.91% and 81.82%, respectively. These findings can be used as a starting point for further investigation using *in vitro* and *in vivo* studies.

**Keywords:** COVID-19, *Nigella sativa* L, molecular docking, SARS-CoV-2

-----  
\*Corresponding author:

Cibinong Science Center, Jl. Raya Bogor Km. 46, Cibinong, Bogor, 16911, Indonesia  
Tel. +62 21 8790 7604, Fax. +62 8790 7612  
E-mail. pamungkasferdian.biochemistry@gmail.com

## Introduction

Severe acute respiratory syndrome coronavirus 2 (SARS-CoV-2) was reported to cause an outbreak in Wuhan, China, in late December 2019. Previously named as 2019-nCoV, this virus causes an unusual respiratory disease, called COVID-19, which is dominated by an initial diagnosis of pneumonia (Zhu *et al.*, 2020). SARS-CoV-2 is the seventh member of the Coronaviridae family of coronaviruses that infect humans (Sun *et al.*, 2020). Currently, there are no drugs, vaccines, or specific antiviral agents available for prevention or treatment of SARS-CoV-2 infection.

Drug research and development for COVID-19 target several parts of the virus that contribute to the infection process, such as spike protein, envelope protein, membrane protein, proteases, nucleocapsid protein, hemagglutinin esterase, helicase, and RNA-dependent RNA polymerase (RdRp) (Prajapat *et al.*, 2020; Wu

*et al.*, 2020). Main protease (Mpro), which is a cysteine protease (Dömling & Gao, 2020) or also called 3-Chymotrypsin like protease (3CLpro), is a promising target for COVID-19 drugs (Sisay, 2020).

The Mpro enzyme from SARS-CoV-2 works to proteolytically cut the overlapping polyproteins pp1a and pp1ab, respectively translated from ORF1a and ORF1b of viral RNA, into functional proteins which release 11 of 13 non-structural proteins (nsp). The important enzymes for replication, such as RdRp or nsp13, will not function properly if there is no release of these proteolytics, i.e. there is no folding and proper assembly into the active polymerase complex. Therefore, inhibition of Mpro activity could terminate the virus life cycle prior to transcription or replication, making Mpro a key enzyme of SARS-CoV-2 viral infection (de Vries *et al.*, 2020; Ullrich & Nitsche, 2020). This indicates

that the enzyme is a potential drug target for SARS-CoV-2.

*Nigella sativa* L. (Ranunculaceae), known as black cumin or black seed, has long been used as a traditional medication to treat various kinds of ailments and disorders (Ahmad *et al.*, 2013). It is native to Southern Europe, North Africa, and Southeast Asia; and is cultivated throughout the world (Khare, 2004). The growing demand of black seed is driven by its wide range of applications, from pharmaceuticals, health supplements, to food ingredients. *N. sativa* is considered as a medicinal plant because it contains bioactive compounds that promote beneficial effects to the human health, such as those having antibacterial, antifungal, antioxidant, anticancer, anti-inflammatory, immunomodulatory effect, cardiovascular-protective, hepato-protective, pulmonary-protective, and anti-asthmatic activities (Ahmad *et al.*, 2013). As with other medicinal plants, this plant is very potential to be explored, as WHO reports that 60–80% of the world's population depend on medicinal herbs as a primary medication (Kadam & Lele, 2017) and as many as 60% of the currently available drugs are derived from plants (Bakal *et al.*, 2017).

The various bioactive compounds in *N. sativa* are reported to include flavonoids, alkaloids, terpenoids, and fatty acids. Those compounds have been demonstrated to carry pharmacological activity against several viral infections, namely those caused by influenza virus H1N1 and anti-HIV type 1 enteroviruses, such as enterovirus-71, poliovirus, chikungunya, echovirus 6, African swine fever virus, coxsackieviruses, hepatitis A, and hepatitis C (Conti *et al.*, 1990; Fan *et al.*, 2011; Hakobyan *et al.*, 2016; Pasetto *et al.*, 2014; Shibata *et al.*, 2014; Sithisarn *et al.*, 2013; Tobergte & Curtis, 2015; Zhang *et al.*, 2014). Nonetheless, antiviral activity of *N. sativa* bioactive compounds against SARS-CoV-2 remains unclear.

*In vitro* and *in vivo* approaches are generally used to obtain information on the effectiveness of an active compound against specific disease, yet these methods are time-consuming and costly. Moreover, they cannot describe how molecular interactions occur in detail. Molecular docking is a tool in structural molecular biology and computer-assisted drug design (*in silico*). The goal of automated

molecular docking software is to understand and predict molecular recognition, both structurally (finding likely binding modes) and energetically (predicting binding affinity). Molecular docking is usually performed between a small molecule (ligand) and a target macromolecule (receptor). It helps to understand drug biomolecular interactions for the rational drug design and discovery (Dar & Mir, 2017; Meng *et al.*, 2012; Schleinkofer *et al.*, 2006). Therefore, this study aims to evaluate the antiviral activity of 24 selected active compounds found in *N. sativa* using molecular docking method with targeted approach. This study also intends to prove that *N. sativa* is potential to be used as a prophylaxis against SARS-CoV-2 infection and also to find a new COVID-19 treatment based on natural products.

## Materials and Methods

### Structures and Computational Tools

The structures used were: (a) the crystal structure of SARS-CoV-2 main protease code 7BQY (Figure 1), (b) active compound ligands from black seed (Table 1), and (c) comparative ligands (Table 2). Computational tools used in this study included hardware tool Asus A409UA-BV351T and the following software tools: AutoDockTools-1.5.6 and AutoDock Vina (Trott & Olson, 2010; Morris *et al.*, 2009), Discovery Studio 2020 Client (DS) (BIOVIA, 2020), LigPlot+ 1.4.5 (Wallace *et al.*, 1995), Open Babel 2.3.1 (O'Boyle *et al.*, 2011s) and ACD/ChemSketch 2016.1 (Advanced Chemistry Development [ACD], 2020).

### Receptor Preparation

The receptor used in the present study was crystal structure of SARS-CoV-2 main protease (code: 7BQY) downloaded from <https://www.rcsb.org/structure/7BQY> in \*PDB file (Figure 1). The receptor was deposited by Liu *et al.* (2020) and studied by Jin *et al.* (2020). The receptor has 1.7 Å resolution and the crystal structure was in complex with inhibitor ligand N3 (N-[(5-Methylisoxazol-3-yl)carbonyl]alanyl-L-valyl-N~1~-(1R,2Z)-4-(benzyloxy)-4-oxo-1-[[3R)-2-oxopyrrolidin-3-yl]methyl]but-2-enyl)-L-leucinamide). The stability of the 7BQY structure was checked using Ramachandran's plot before preparation (Lovell *et al.*, 2003). Preparation was

performed using AutoDockTools-1.5.6 to remove water, ligand and hetero atom attached in the receptor, to add hydrogen atom, and to calculate its Gasteiger charge. The file was then saved as \*PDBQT file and ready to run in molecular docking using AutoDockTools-1.5.6 and AutoDock Vina. The preparation of receptor 7BQY was also done to determine the active site, binding site, and covalent bonding based on the amino acid residues sequence accessed from <https://www.rcsb.org/sequence/7BQY>.

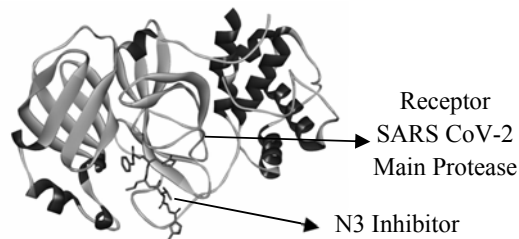


**Figure 1.** Crystal structure of SARS-CoV-2 main protease (Code:7BQY) in 3D conformation.

### Ligand Preparation

The ligands used in this study consist of 24 active compounds found in *N. sativa* based on LC/MS analysis by Kadam & Lele (2017) and a review by Ahmad *et al.* (2013) (Table 1). In addition, chloroquine, hydroxychloroquine, favipiravir, and remdesivir (Table 2) were used as comparative ligands due to their previously reported have antiviral activity (Costanzo *et al.*, 2020). These four drugs have been given to several COVID-19 patients having severe symptoms. Takahashi *et al.* (2020) showed that improved clinical respiratory symptoms were observed following the administration of favipiravir to three COVID-19 patients. One patient in the United States was given remdesivir on the 11th day since onset and gave a gradually improving response to clinical symptoms (Cao *et al.*, 2020). However, the antiviral activity of these four compounds has not been reported to be specifically related to Mpro of SARS-CoV-2, but several *in silico* studies have also been conducted on these compounds to target Mpro (da Silva Arouche *et al.*, 2020; Narkhede *et al.*, 2020).

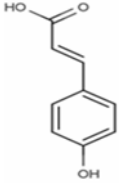
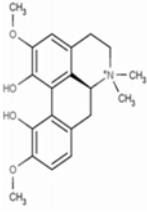
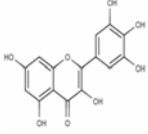
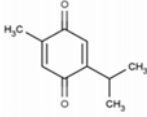
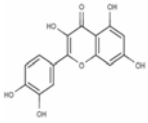
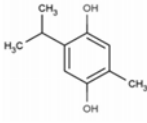
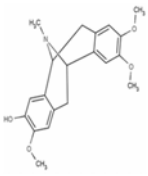
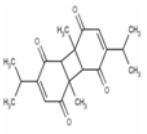
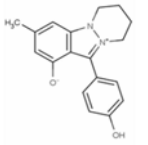
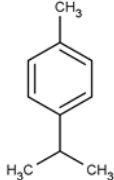
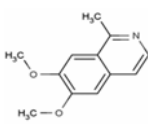
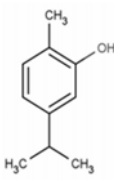
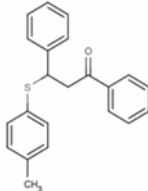
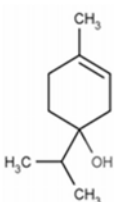
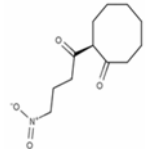
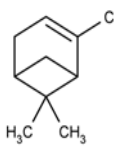
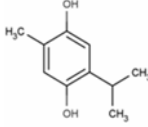
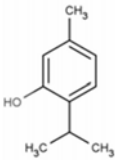
Ligand N3 that was in complex with the SARS CoV-2 crystal structure 7BQY (Jin *et al.*, 2020; Liu *et al.*, 2020) was also used as a reference area. All ligands were reconstructed

using ACD/ChemSketch 2016.1 and saved as \*.mol file. The \*.mol files were then converted into \*.PDB file using OpenBabel (O'Boyle *et al.*, 2011). The \*.PDB file was then converted into \*.PDBQT file using AutoDockTools-1.5.6. and ready to be run in the molecular docking simulation.

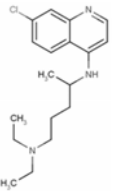
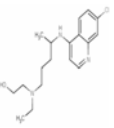
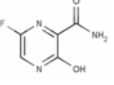
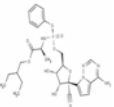
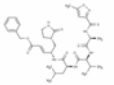
All selected ligands were analyzed for their solubility and toxicity. The solubility analysis was carried out by using Lipinski's Rule of Five at pH = 7, which can be accessed on <http://scfbio-iitd.res.in/software/drugdesign/lipinski.jsp> (Lipinski *et al.*, 2012). The toxicity analysis was conducted using admetSAR simulation, which can be accessed on <http://lmmd.ecust.cn:8000/predict/> (Cheng *et al.*, 2012).

**Table 1.** Ligand structures of selected active compounds from *N. sativa*

Ligand	Molecular Formula	2D Structure	MW (g/mol)
Kaempferol	C <sub>15</sub> H <sub>10</sub> O <sub>6</sub>		286
Apigenin	C <sub>15</sub> H <sub>10</sub> O <sub>5</sub>		270
Biochanin a	C <sub>16</sub> H <sub>12</sub> O <sub>5</sub>		284
Limonen-6-ol, pivalate	C <sub>15</sub> H <sub>24</sub> O <sub>2</sub>		236
β-Pinene	C <sub>10</sub> H <sub>16</sub>		136
Pyrrolidin-2-one	C <sub>4</sub> H <sub>7</sub> NO		85

p-Coumaric acid	$C_9H_8O_3$		164	Magnoflorine	$C_{20}H_{24}NO_4$		342
Myricetin	$C_{15}H_{10}O_8$		318	Thymoquinone	$C_{10}H_{12}O_2$		164
Quercetin	$C_{15}H_{10}O_7$		302	Thymohydroquinone	$C_{10}H_{14}O_2$		166
Norargemone	$C_{20}H_{23}NO_4$		341	Dithymoquinone	$C_{20}H_{24}O_4$		328
Nigellidine	$C_{18}H_{18}N_2O_2$		294	p-Cymene	$C_{10}H_{14}$		138
Nigellimine	$C_{12}H_{13}NO_2$		203	Carvacrol	$C_{10}H_{14}O$		150
3-[(4-Methylphenyl)sulfanyl]-1,3-diphenyl-1-propanone	$C_{22}H_{20}OS$		334	4-Terpinol	$C_{10}H_{18}O$		154
2-(4-Nitrobutyryl)cyclooctanone	$C_{12}H_{19}NO_4$		241	α-Pinene	$C_{10}H_{16}$		136
Thymoquinol	$C_{10}H_{14}O_2$		166	Thymol	$C_{10}H_{14}O$		150

**Table 2.** Structures of comparative ligands

Ligand	Molecular Formula	2D Structure	MW (g/mol)
Chloro-quine	C <sub>18</sub> H <sub>26</sub> ClN <sub>3</sub>		319.50
Hydroxy-chloroquine	C <sub>18</sub> H <sub>26</sub> ClN <sub>3</sub> O		335.50
Favipiravir	C <sub>5</sub> H <sub>4</sub> FN <sub>3</sub> O <sub>2</sub>		157.00
Remdesivir	C <sub>27</sub> H <sub>35</sub> N <sub>6</sub> O <sub>8</sub> P		602.00
N3	C <sub>35</sub> H <sub>48</sub> N <sub>6</sub> O <sub>8</sub>		680.79

### Molecular Docking Simulation

Molecular docking simulation was performed using AutoDockTools 1.5.6 and AutoDock Vina with a site directed approach. The area and coordinates were determined following the position of the initial ligand N3 attached on the crystal structure of SARS-CoV-2 main protease 7BQY. The center of coordinate had been set to X = 10.398, Y = -1.254, and Z = 23.473 while the grid size had been set to X= 40, Y = 46, and Z = 40. The present study set exhaustiveness = 64 and num modes = 20 to increase the accuracy. Num modes represent the number of interaction models after molecular docking simulation.

AutoDockTools 1.5.6 and AutoDock Vina were validated by redocking the initial ligand N3 which was previously in complex with receptor crystal structure 7BQY. The programs are stated to be valid if the initial ligand N3 occupied the same area after redocked or with root mean square of deviation (RMSD) of less than 2.5 Å (Baber *et al.*, 2009). The validation result, as seen on Figure 2, shows that the ligand N3 occupied the same area which indicates that the programs are valid and can be used for the

molecular docking simulation. Both selected black seed ligands and comparative ligands were simulated in the same coordinates, grid size, exhaustiveness, and num modes on the crystal structure 7BQY using AutoDockTools 1.5.6 and AutoDock Vina. The molecular docking simulation resulted in the binding affinity energy ( $\Delta G$ ) data and docked structure data in \*PDBQT form. The docked structure data was then analyzed and visualized using Ligplot 1.4.5 and DS Client to show the binding site and bonding type that were resulted from the molecular docking simulation.

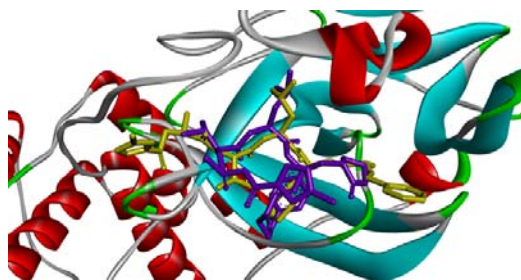


**Figure 2.** Visualization of 3D docking validation: the initial inhibitor ligand N3 (yellow) and after redocking (purple).

### Results

#### Structure and Stability of the Receptor

The stability of the receptor structure can be determined by its resolution and Ramachandran's plot. The receptor is said to be stable and can be used for molecular docking simulation if the receptor has a resolution of less than 2.5 Å (Lu *et al.*, 2009). Moreover, the receptor is said to be in a stable state if the amino acid residues on Ramachandran's plot which occupy the disallowed region are less than 15% (Ho & Brasseur, 2005). The receptor SARS-CoV-2 Mpro code 7BQY has a resolution of 1.7 Å and the number of amino acid residues which fill the disallowed region on Ramachandran's plot are 0% (Figure 3). The data showed that the receptor 7BQY is in a stable state and can be used in molecular docking simulation.

The receptor 7BQY consists of 306 amino acid residues. Based on the sequence data from <https://www.rcsb.org/sequence/7BQY>, the residue involved in covalent bond formation is Cys145, while those involved in the active site formation are His41 and Cys145. The

residues involved in binding site formation are Thr26, Leu27, Phe140, Met142, Gly143, Cys145, His163, His164, Glu166, His172. These 11 residues are potential to interact with any ligands and could possibly affect the function of the enzyme Mpro 7BQY. These 11 amino acids in the present study were used to determine the percentage of occupancy of the ligand.

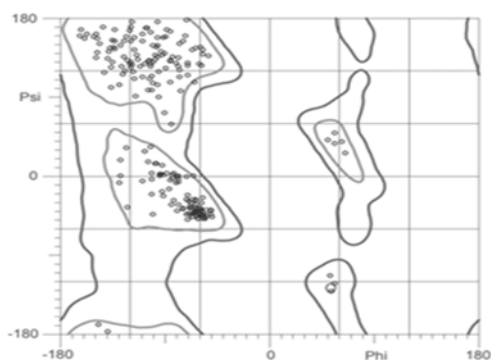


**Figure 3.** Ramachandran's plot of receptor 7BQY: 98.3% (295/300) of all residues were in the favoured regions (inside light lines); 100.0% (300/300) of all residues were in the allowed regions (inside dark lines) (Analysis of Ramachandran's plot was carried out in an online application, MolProbity (Prisant *et al.*, 2020) which is available at <http://molprobity.biochem.duke.edu/index.php?MolProbSID=k7t41ngp2o2kmb4tpfi4d0amf0&eventID=62> [accessed on October 29th, 2020]).

### The Lipinski and Solubility Analysis of the Ligands

Lipinski's Rule of Five requires a compound to comply with all of the following: molecular weight (MW) of less than 500 g/mol, a Log P value of less than 5, hydrogen bond donors (HBDs) of no more than 5, and hydrogen bond acceptors (HBAs) of no more than 10. In addition, two supplementary rules were recommended in further studies, which are a polar surface area (PSA) of at most 140 Å and rotatable bonds (Rot B) of less than 10 (Chen *et al.*, 2020). However, assessment in this study used four parameters, which are molecular weight, hydrogen bond donor, hydrogen bond acceptor, and log P.

Table 3 shows that the molecular weight (MW) of all ligands fall between 85-602 g/mol, their numbers of hydrogen bond donors (HBDs) fall between 0 – 6, their numbers of hydrogen bond acceptors (HBAs) fall between 0 – 13, and

the Log P values fall between -2.61 – 2.58. From these results, it can be deduced that all the tested ligands followed the four rules of Lipinski's, except for myricetin and remdesivir that followed only three out of four rules. Myricetin has more than five hydrogen bond donors (HBDs), while remdesivir has molecular weight of more than 500 g/mol and more than 10 hydrogen bond acceptors (HBAs).

**Table 3.** Solubility of the ligands using Lipinski's rules

Ligand	MW (g/mol)	HBD	HBA	Log P	Lipinski Result
Kaempferol	286	0	6	-1.51	yes
Apigenin	270	3	5	-1.00	yes
Biochanin a	284	2	4	-1.11	yes
Limonen-6-ol, pivalate	236	0	2	0.85	yes
β-Pinene	136	0	0	0.63	yes
Pyrrolidin-2-one	85	1	2	-0.14	yes
p-Coumaric acid	164	2	3	-2.02	yes
Myricetin	318	6	8	-2.61	yes (3/4)
Quercetin	302	5	7	-1.95	yes
Norargemone	341	1	5	1.61	yes
Nigellidine	294	0	2	-1.08	yes
Nigellimine	203	0	3	1.05	yes
3-[(4-Methylphenyl)sulfanyl]-1,3-diphenyl-1-propanone	334	0	1	2.58	yes
2-(4-Nitrobutyryl)cyclooctanone	241	0	4	-0.49	yes
Thymoquinol	166	0	2	-0.37	yes
Magnoflorine	342	0	4	1.46	yes
Thymoquinone	164	0	2	-0.37	yes
Thymohydroquinone	166	0	2	-0.13	yes
Dithymoquinone	328	0	4	-0.48	yes
p-Cymene	134	0	0	1.03	yes
Carvacrol	150	0	1	0.22	yes
4-Terpeneol	154	0	1	0.09	yes
α-Pinene	136	0	0	0.63	yes
Thymol	150	0	1	0.06	yes
Chloroquine	319,5	0	3	0.49	yes

Hydroxy-chloroquine	335,5	0	4	-0.34	yes
Favipiravir	157	0	5	-0.81	yes
Remdesivir	602	0	13	1.99	yes (3/4)

### The admetSAR and Toxicity Analysis of the Ligands

All ligands tested by admetSAR showed non-carcinogenic properties, but the carcinogenicity (trinary) of p-Cymene was found as “warning” in low accuracy (less than 75%) (Table 4). Among 29 ligands, 14 were categorized as non-hepatotoxic in various accuracy scores and five ligands were categorized based on U.S. EPA as type II in acute oral toxicity, which means that they are moderately toxic. These were kaempferol, myricetin, quercetin, thymoquinone, and chloroquine. Meanwhile, the others were categorized as type III, which meant non-toxic (slightly toxic) (Guan *et al.*, 2018; Li *et al.*, 2014).

**Table 4.** Toxicity using admetSAR

Ligand	Carcinogenicity		Toxicity		
	Binary	Trinary	Hepar	Acute Oral (c)	Acute Oral (kg/mol)
Kaempferol	- (1.00)	NR (0.70)	+	II (0.62)	1.74
Apigenin	- (1.00)	NR (0.60)	+	III (0.70)	1.15
Biochanin a	- (1.00)	NR (0.62)	+	III (0.70)	1.82
Limonen-6-ol, pivalate	- (0.67)	NR (0.58)	-	III (0.81)	1.68
β-Pinene	- (0.73)	NR (0.48)	-	III (0.83)	1.41
Pyrrolidin-2-one	- (0.89)	NR (0.59)	-	III (0.49)	2.05
p-Coumaric acid	- (0.79)	NR (0.60)	-	III (0.49)	2.00
Myricetin	- (1.00)	NR (0.68)	+	II (0.72)	2.38
Quercetin	- (1.00)	NR (0.68)	+	II (0.73)	2.56
Norargemone	- (1.00)	NR (0.61)	+	III (0.70)	1.14

Nigellidine	- (0.90)	NR (0.54)	+	III (0.52)	1.98
Nigellimine	- (0.94)	NR (0.54)	+	III (0.46)	1.53
3-[(4-Methylphenyl)sulfonyl]-1,3-diphenyl-1-propanone	- (0.76)	NR (0.59)	+	III (0.87)	1.85
2-(4-Nitrobutyryl)cyclooctanone	- (0.79)	NR (0.61)	-	III (0.66)	2.03
Thymoquinol	- (0.53)	NR (0.72)	-	III (0.84)	2.17
Magnoflorine	- (1.00)	NR (0.71)	+	III (0.68)	1.87
Thymoquinone	- (0.67)	NR (0.60)	-	II (0.68)	1.29
Thymohydroquinone	- (0.53)	NR (0.72)	-	III (0.84)	2.17
Dithymoquinone	- (0.76)	NR (0.45)	+	III (0.45)	2.18
p-Cymene	- (0.51)	W (0.56)	-	III (0.84)	1.88
Carvacrol	- (0.53)	NR (0.72)	-	III (0.84)	2.53
4-Terpineol	- (0.84)	NR (0.60)	-	III (0.82)	2.05
α-Pinene	- (0.73)	NR (0.47)	-	III (0.83)	1.53
Thymol	- (0.53)	NR (0.72)	-	III (0.84)	2.20
Chloroquine	- (0.83)	NR (0.68)	+	II (0.74)	2.68
Hydroxychloroquine	- (0.84)	NR (0.65)	-	III (0.45)	2.67
Favipiravir	- (0.87)	NR (0.75)	+	III (0.54)	1.41
Remdesivir	- (0.97)	NR (0.54)	+	III (0.54)	3.73
N3	- (0.79)	NR (0.52)	-	III (0.62)	2.89

Notes: The values inside the bracket sign ( ) are the accuracy scores with the highest score being 1.00; NR= non-required; W= warning.

### The Affinity Energy of Gibbs

Molecular docking simulation showed that 10 out of 24 active compounds from *N. sativa* (dithymoquinone, magnoflorine, 3-[(4-Methylphenyl)sulfanyl]-1,3-diphenyl-1-propanone, nigellidine, norargemonine, myricetin, quercetin, biochanin a, apigenin, and kaempferol) and remdesivir (as a synthetic comparative ligand) have lower affinity energy than N3 inhibitor (Figure 4). The lower affinity energy (as shown by a more negative value) means it can bind stronger to the receptor.

The result of the other docking study conducted by da Silva Arouche *et al.*, (2020) on pharmacological inhibitor compounds with Mpro having a different PDB ID, 6LU7, showed that it had a lower N3 affinity energy (-10.1 kcal/mol) than this study. Their study showed that chloroquine had the lowest affinity energy value of -10.8 kcal/mol, but it was not too different from the N3 affinity energy they redocked. Our study obtained the lowest pharmacological comparison on the inhibitor affinity energy for remdesivir with a value of 1.3 times than N3. In contrast, their study found the inhibitor affinity energy value to be 1.3 times lower than their redocking N3. In addition, the study conducted by Narkhede *et al.*, (2020) reported that the affinity energy of remdesivir for Mpro 6LU7 was previously found to be higher at -6.5 kcal/mol, meaning that the bond was ~1.3 times weaker than the results of this study. The differences in the affinity energy values might be caused by different conformational position between both Mpro 6LU7 and 7BQY and exhaustiveness that was applied in the molecular docking simulation.

### Binding Analysis

Molecular docking simulation showed that the N3 inhibitor was able to bind to 21 residues, namely Glu166, Cys145, Ser46, Gln189, Arg188, Gly143, Ser144, Asn142, Leu141, Leu27, Phe140, His172, His163, Leu167, Thr190, Met165, Met49, Tyr54, His41, Asp187, and His164 based on DS analysis (Figure 6a). This inhibitor also binds to 15 residues including Cys145, Gly143, Phe140, Asn142, His163, Leu141, Met165, His164, His41, Tyr54, Asp187, Thr190, Ser46, Gln189, and Glu166 based on Ligplot analysis (Figure 6b). The binding similarity of all ligands were calculated based on these amino acid residues of N3 inhibitors. The result showed that 3-[(4-Methylphenyl)sulfanyl]-1,3-diphenyl-1-propanone and remdesivir were the most

similar to N3 (Table 5). The 3D interaction between Mpro with 3-[(4-Methylphenyl)sulfanyl]-1,3-diphenyl-1-propanone and remdesivir is shown in Figure 5. The binding analysis using Ligplot and DS on 2D interaction of 3-[(4-Methylphenyl)sulfanyl]-1,3-diphenyl-1-propanone and remdesivir are shown in Figure 7 and Figure 8, respectively. The binding analysis also determined the occupancy percentage based on the active site, binding site, and covalent binding taken from protein sequence of Mpro 7BQY. The highest occupancy value belonged to 3-[(4-Methylphenyl)sulfanyl]-1,3-diphenyl-1-propanone and remdesivir, obtained from both Ligplot and DS analysis (Table 5).

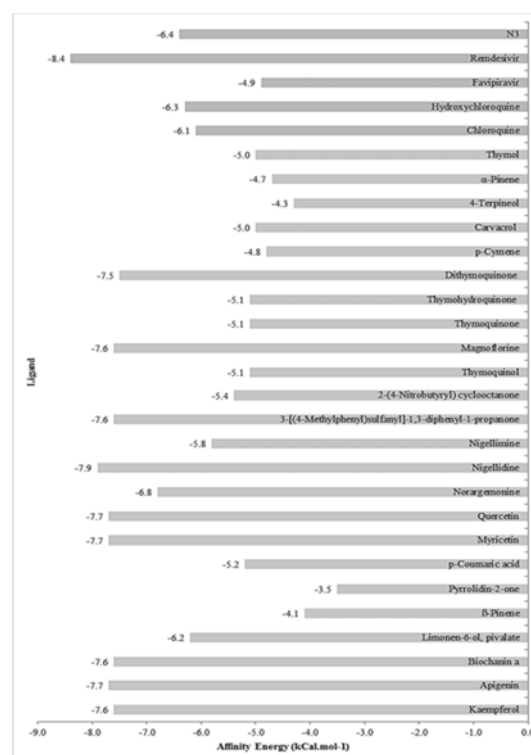


**Figure 4.** Affinity energy of ligands interacting with Mpro (code: 7BQY).

**Table 5.** The binding similarity towards N3 inhibitor and the binding occupancy towards binding sites on receptor sequence



Ligand	Similarity Based on N3 Inhibitor (%)		Occupancy Based on Active Site, Binding Site, and Covalent Binding (%)	
	LP	DS	LP	DS
N3	100	100	72.73	90.91
Kaempferol	46.67	47.62	27.27	27.27
Apigenin	66.67	66.67	54.55	54.55
Biochanin a	80.00	66.67	63.64	63.64
Limonen-6-ol, pivalate	73.33	71.43	63.64	72.73
β-Pinene	53.33	52.38	63.64	72.73
Pyrrolidin-2-one	33.33	38.10	18.18	18.18
p-Coumaric acid	33.33	38.10	18.18	27.27
Myricetin	46.67	47.62	27.27	27.27
Quercetin	46.67	47.62	27.27	27.27
Norargemone	46.67	52.38	54.55	72.73
Nigellidine	46.67	57.14	36.36	54.55
Nigellimine	46.67	47.62	27.27	36.36
3-[(4-Methylphenyl)sulfonyl]-1,3-diphenyl-1-propanone	86.67	76.19	90.91	81.82
2-(4-Nitrobutyl)cyclo-octanone	53.33	66.67	45.45	81.82
Thymoquinol	40.00	42.86	27.27	27.27
Magnoflorine	53.33	52.38	36.36	45.45
Thymoquinone	46.67	42.86	27.27	36.36
Thymohydroquinone	40.00	47.62	27.27	27.27

Dithymoquinone	46.67	42.86	27.27	27.27
p-Cymene	40.00	38.10	27.27	27.27
Carvacrol	46.67	42.86	27.27	27.27
4-Terpineol	33.33	42.86	18.18	27.27
α-Pinene	40.00	38.10	18.18	18.18
Thymol	40.00	38.10	27.27	27.27
Chloroquine	66.67	66.67	45.45	54.55
Hydroxychloroquine	66.67	66.67	45.45	54.55
Favipiravir	40.00	38.10	18.18	27.27
Remdesivir	73.33	76.19	63.64	81.82

Notes: LP= Ligplot analysis; DS= Discovery Studio analysis.

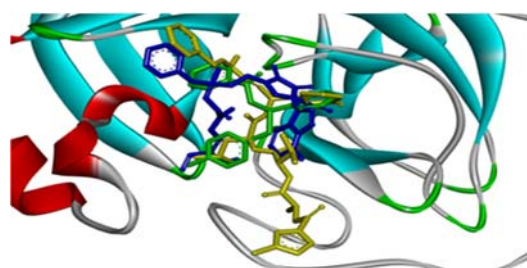


**Figure 5.** Interaction between Mpro and 3-[(4-Methylphenyl)sulfonyl]-1,3-diphenyl-1-propanone (green) and remdesivir (blue) compared to N3 (yellow).

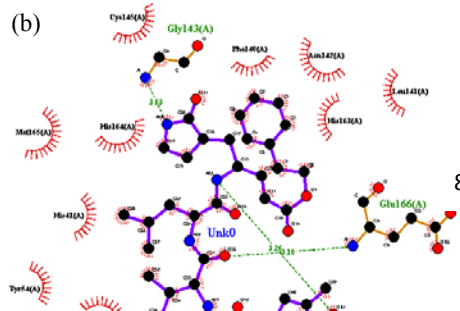
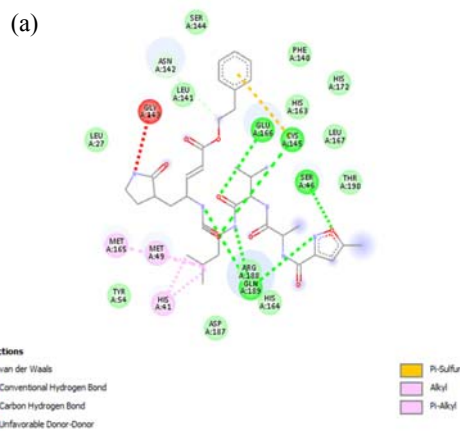


**Figure 6.** The 2D interaction between Mpro and N3 inhibitor using DS (a) and Ligplot (b).

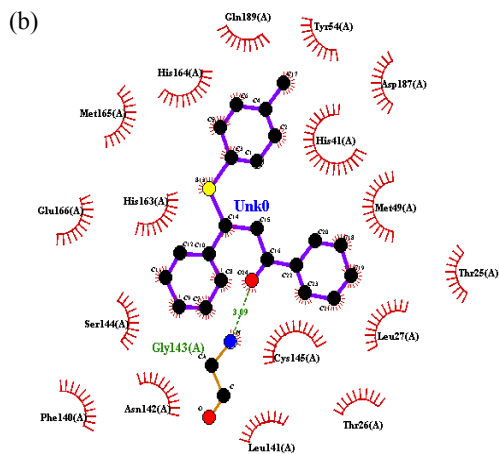
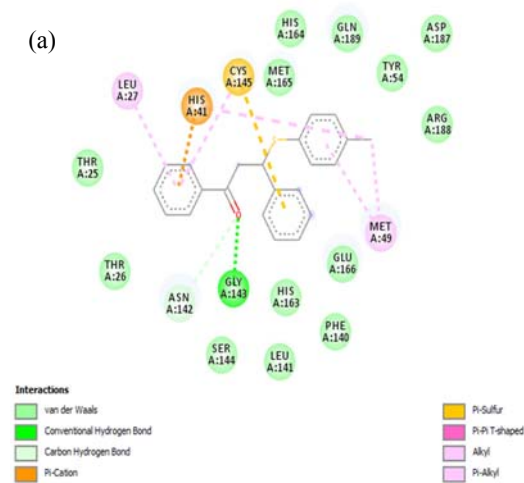


**Figure 7.** The 2D interaction between Mpro and 3-[(4-Methylphenyl)sulfonyl]-1,3-diphenyl-1-propanone using DS (a) and Ligplot (b).

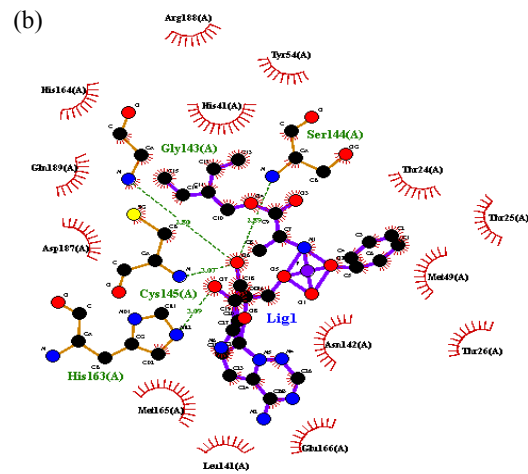
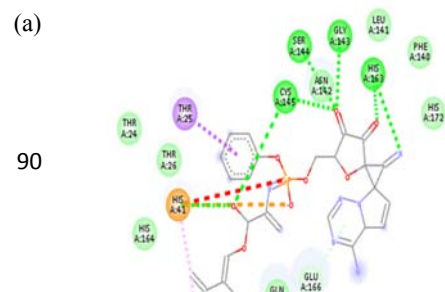


**Figure 8.** The 2D interaction between Mpro and remdesivir using DS (a) and Ligplot (b).

## Discussion

In this *in silico* study, we targeted the main protease (Mpro, also known as 3CLpro) from SARS-CoV-2 to obtain a molecule/ligand from *N. sativa* (black seed) as a potential COVID-19 drug. This Mpro proteolytically cuts the polypeptide resulted from translation after the virus has successfully entered the target cell to replicate (Huang *et al.*, 2020). The target molecule we used is Mpro code 7BQY with N3 inhibitor of SARS-CoV-2 (Liu *et al.*, 2020). This receptor has a resolution of 1.7 Å, which indicates that the molecule has a stable structure.

Another study using Mpro as the target receptor to bind with only nine potential ligands from *N. sativa* (Salim & Nouredine, 2020), whereas 24 ligands were used in this study

(Ahmad *et al.* 2013; Kadam & Lele, 2017). The same study only used the binding affinity parameter to obtain the results (Salim & Noureddine, 2020), while in this study also determine similarity compared to N3 and occupancy based on the residues of the active sites, the binding sites, and the covalent bond that were obtained from the secondary structure of 7BQY in <https://www.rcsb.org/sequence/7BQY>. The similarity with N3 was determined based on the amino acids residues that interacted with N3 after redocking. The occupancy refers to the residues involved in the formation of active site and binding site. The residues that can form covalent bond to determine the occupancy were also considered, as the covalent bond is a strong bond that forms tertiary structure of the protein (in this case the Cys145 has -SH group on its R-group that can form covalent bond, namely disulphide interaction). Moreover, the residue which can form covalent bonds is crucial for interaction with the ligand because the functional group on the covalent bond is relatively more reactive.

Based on the Ramachandran's plot, no residues from Mpro 7BQY were found outside the allowable area (Figure 3). It shows that this secondary structure of the protein is stable, so it is predicted that it will not interfere with the molecular docking analysis to be carried out.

The solubility and toxicity of all ligands used in this study were evaluated, including four comparative compounds reported to have antiviral activity (Costanzo *et al.*, 2020). Solubility properties of the ligands were screened using four variables of Lipinski's Rule of Five. The Rule of Five predict that a ligand is more likely to have a good absorption when it meets these conditions: HBDs are less than 5, HBAs are less than 10. MW is lower than 500 g/mol, and Log P is lower than 5 (Lipinski *et al.*, 2012). Of all screened ligands, myricetin and remdesivir were predicted to have the lowest solubility, since they only follow three variables. In other words, the high number of HBDs in myricetin and high MW and HBAs in remdesivir could hinder the permeability across the bilayer membrane.

Toxicity properties were evaluated to predict the carcinogenicity and acute oral toxicity of the ligands using AdmetSAR tool. The data results were equipped with an accuracy score. All screened ligands were predicted as non-carcinogenic, both in binary and ternary. In spite of p-Cymene being predicted as "warning"

for the ternary carcinogenicity, its low accuracy (0.5585) may cause it unlikely to be addressed, yet the status remains noticeable. The acute oral toxicity was divided into four categories: category I ( $LD50 \leq 50$  mg/kg) and category II ( $50$  mg/kg  $< LD50 \leq 500$  mg/kg) were considered as toxic, while category III ( $500$  mg/kg  $< LD50 \leq 5000$  mg/kg) and category IV ( $5000$  mg/kg  $< LD50$ ) were considered to be non-toxic (Guan *et al.*, 2018). Kaempferol, myricetin, quercetin, thymoquinone, and chloroquine were predicted to be in the category II, while the others in the category III. Toxicity prediction provided a cautionary information before using these five ligands for further research or application, since they were considered as toxic while the other ligands were relatively safe to be used.

The molecular docking simulation was performed using 24 ligands from *N. sativa*, four comparative ligands, and one N3 inhibitor as a reference ligand. The N3 inhibitor was used to determine the center and area of molecular docking simulation. We hypothesised that the tested ligand can be strongly predicted as an Mpro inhibitor as long as it has more negative affinity energy than N3 inhibitor and high similarity in residue binding compared to N3 inhibitor. There were 10 ligands (dithymoquinone, magnoflorine, 3-[(4-Methylphenyl)sulfanyl]-1,3-diphenyl-1-propanone, nigellidine, norargemonine, myricetin, quercetin, biochanin a, apigenin, and kaempferol) from the black seed that have more negative affinity energy, whereas only one comparative ligand, remdesivir, which has more negative affinity energy. In addition, we found that only 3-[(4-Methylphenyl)sulfanyl]-1,3-diphenyl-1-propanone was the most consistent ligand having high similarity as analysed by Ligplot (86.67%) and DS (76.19%). We also found that remdesivir has high similarity toward N3 inhibitor as analysed by Ligplot (73.33%) and DS (76.19%).

The binding analysis performed to analyze the percentage of occupancy based on the active site, the binding site, and the covalent bond of the receptor Mpro 7BQY revealed that 3-[(4-Methylphenyl)sulfanyl]-1,3-diphenyl-1-propanone also consistently showed high occupancy percentage on the Ligplot and DS analysis, with the value of 90.91% and 81.82% respectively. In contrast, remdesivir showed inconsistent occupancy percentage using

Ligplot and DS analysis, with 63.64% and 81.82% values, respectively.

Collectively, eventhough the *in silico* study only resulting a prediction, the results of this present study suggested that 3-[(4-Methylphenyl)sulfanyl]-1,3-diphenyl-1-propanone as the most potent ligand from *N. sativa* that can inhibit SARS-CoV-2 Mpro based on the energy affinity, binding similarity towards the N3 inhibitor, and the occupancy percentage. Moreover, this ligand also has good solubility and permeability properties, and is non-carcinogenic and non-toxic. Compared to remdesivir, this active compound was better as it also had higher similarity and occupancy percentage. Deeper investigation through *in vitro* and *in vivo* studies are needed to prove that the 3-[(4-Methylphenyl)sulfanyl]-1,3-diphenyl-1-propanone can inhibit SARS-CoV-2 Mpro.

All selected ligands from *N. sativa* and four comparative ligands were successfully docked on the receptor SARS-CoV-2 Mpro 7BQY, as indicated by the negative value of affinity energy ( $\Delta G$ ). However, the 3-[(4-Methylphenyl)sulfanyl]-1,3-diphenyl-1-propanone had the highest similarity and occupancy when compared to the other selected *N. sativa* ligands and to remdesivir, while remdesivir had the highest similarity and occupancy when compared to the other comparative ligands. This study suggested that 3-[(4-Methylphenyl)sulfanyl]-1,3-diphenyl-1-propanone is the most potent *N. sativa* ligand to inhibit receptor SARS-CoV-2 Mpro out of the 24 ligands tested. Binding energy was evaluated after the redocked N3 showed the exact same position to its original crystal structure.

## Conflicts of Interest

The authors declare that there is no conflicts of interest regarding the publication of this paper and all authors equally contributed to this paper.

## References

Advanced Chemistry Development Inc. [ACD]. (2020). *ACD/ChemSketch, version 2016.1*. Toronto, ON, Canada. Retrieved from [www.acdlabs.com](http://www.acdlabs.com).

- Ahmad, A., Husain, A., Mujeeb, M., Khan, S.A., Najmi, A. K., Siddique, N. A., Damanhour, Z. A., & Anwar, F. (2013). A Review on Therapeutic Potential on *Nigella sativa*: A Miracle Herb. *Asian Pacific Journal of Tropical Biomedicine*, 3(5), 337–352. doi: 10.1016/S2221-1691(13)60075-1
- Baber, J.C., Thompson, D.C., Cross, J.B., & Humblet, C. (2009). GARD: A Generally Applicable Replacement for RMSD. *Journal of Chemical Information and Modeling*, 49(8), 1889–1900. doi: 10.1021/ci9001074
- Bakal, S.N., Bereswill, S., & Heimesaat, M.M. (2017). Finding Novel Antibiotic Substances from Medicinal Plants — Antimicrobial Properties of *Nigella sativa* Directed Against Multidrug Resistant Bacteria. *European Journal of Microbiology and Immunology*, 7(1), 92–98. doi: 10.1556/1886.2017.00001
- BIOVIA. (2020). Dassault Systèmes, [Discovery Studio], [2020 Client], San Diego: Dassault Systèmes.
- Cao, Y. Deng, Q., Dai, S. (2020). Remdesivir for severe acute respiratory syndrome coronavirus 2 causing COVID-19: an evaluation of the evidence. *Travel Medicine and Infectious Disease*, 35, 101647. doi: 10.1016/j.tmaid.2020.101647
- Chen, X., Li, H., Tian, L., Li, Q., Luo, J., & Zhang, Y. (2020). Analysis of the Physicochemical Properties of Acaricides Based on Lipinski's Rule of Five. *Journal of Computational Biology*, 27(0), 1–10. <https://doi.org/10.1089/cmb.2019.0323>
- Cheng, F., Li, W., Zhou, Y., Shen, J., Wu, Z., Liu, G., Lee, P. W., & Tang, Y. (2012) AdmetSAR: A Comprehensive Source and Free Tool for Assessment of Chemical ADMET Properties. *Journal of Chemical Information and Modeling*, 52(11), 3099–3105. doi: 10.1021/ci300367a
- Conti, C., Genovese, D., Santoro, R., Stein, M.L., Orsi, N., & Fiore, L. (1990). Activities and Mechanisms of Action of Halogen-Substituted Flavanoids Against Poliovirus Type 2 Infection In Vitro. *Antimicrobial Agents and Chemotherapy*, 34(3), 460–466. doi: 10.1128/AAC.34.3.460
- Costanzo, M., De Giglio, M.A.R., & Roviello, G.N. (2020). SARS CoV-2: Recent Reports on Antiviral Therapies Based on Lopinavir/Ritonavir, Darunavir/Umifenovir, Hydroxychloroquine, Remdesivir, Favipiravir and Other Drugs for the Treatment of the New Coronavirus. *Current Medicinal Chemistry*, 27(27). doi: 10.2174/0929867327666200416131117
- da Silva Arouche, T., Reis, A.F., Martins, A.Y., Costa, J.F.S., Junior, R.N.C., Neto, A.M.J.C. (2020). Interactions between remdesivir, ribavirin, favipiravir, galidesivir,

- hydroxychloroquine and chloroquine with fragment molecular of the COVID-19 main protease with inhibitor N3 complex (PDB ID:6LU7) using molecular docking. *Journal of Nanoscience and Nanotechnology*, 20, 7311-7323. doi: 10.1166/jnn.2020.18955
- Dar, A.M., & Mir, S. (2017). Molecular Docking: Approaches, Types, Applications and Basic Challenges. *Journal of Analytical & Bioanalytical Techniques*, 8(2), 1000356. doi: 10.4172/2155-9872.1000356
- de Vries, M., Mohamed, A.S., Prescott, R.A., Valero-Jimenez, A.M., Desvignes, L., O'Connor, R., Steppan, C., Anderson, A.S., Binder, J., & Dittmann, M. (2020). Comparative study of a 3CLpro inhibitor and remdesivir against both major SARS-CoV-2 clades in human airway models. *bioRxiv*. doi: 10.1101/2020.08.28.272880
- Fan, D., Zhou, X., Zhao, C., Chen, H., Zhao, Y., & Gong, X. (2011). Anti-Inflammatory, Antiviral and Quantitative Study of Quercetin-3-O- $\beta$ -D-Glucuronide in *Polygonum perfoliatum* L. *Fitoterapia*, 82(6), 805–810. doi: 10.1016/j.fitote.2011.04.007
- Guan, L., Yang, H., Cai, Y., Sun, L., Di, P., Li, W., Liu, G., & Tang, Y. (2018). ADMET-score - A Comprehensive Scoring Function for Evaluation of Chemical Drug-Likeness. *Medchemcomm*, 10(1), 148-157. doi:10.1039/c8md00472b
- Hakobyan, A., Arabyan, E., Avetisyan, A., Abroyan, L., Hakobyan, L., & Zakaryan, H. (2016). Apigenin Inhibits African Swine Fever Virus Infection In Vitro. *Archives of Virology*, 161(12), 3445–3453. doi: /10.1007/s00705-016-3061-y
- Ho, B. K., & Brasseur, R. (2005). The Ramachandran Plots of Glycine and Pre-Proline. *BMC Structural Biology*, 5, 14. doi: 10.1186/1472-6807-5-14
- Huang, Y., Yang, C., Xu, X., Xu, X., & Liu, S. (2020). Structural and Functional Properties of SARS-CoV-2 Spike Protein: Potential Antivirus Drug Development for COVID-19. *Acta Pharmacologica Sinica*, 0, 1-9. doi: 10.1038/s41401-020-0485-4
- Jin, Z., Du, X., Xu, Y., Deng, Y., Liu, M., Zhao, Y., Zhang, B., Li, X., Zhang, L., Peng, C., Duan, Y., Yu, J., Wang, L., Yang, K., Liu, F., Jiang, R., Yang, X., You, T., Liu, X., Yang, X., Bai, F., Liu, H., Liu, X., Guddat, L. W., Xu, W., Xiao, G., Qin, C., Shi, Z. Jiang, H., Rao, J., & Yang, H. (2020). Structure of M<sup>pro</sup> from SARS-CoV-19 and Discovery of Its Inhibitors. *Nature*, 582, 289-293. doi: 0.1038/s41586-020-2223-y
- Kadam, D., & Lele, S. S. (2017). Extraction, Characterization and Bioactive Properties of *Nigella sativa* Seedcake. *Journal of Food Science and Technology*, 54(12), 3936–3947. doi: 10.1007/s13197-017-2853-8
- Khare, C. P. (2004). *Encyclopedia of Indian medicinal plants*. New York, US: Springes-Verlag Berlin Heidelberg.
- Li, X., Chen, L., Cheng, F., Wu, Z., Bian, H., Xu, C., Li, W., Liu, G., Shen, X., & Tang, Y. (2014). In Silico Prediction of Chemical Acute Oral Toxicity Using Multi-Classification Methods. *Journal of Chemical Information and Modelling*, 54, 1061–1069. doi: 10.1021/ci5000467
- Lipinski, C. A., Lombardo, F., Dominy, B. W., & Feeney, P. J. (2012). Experimental and Computational Approaches to Estimate Solubility and Permeability in Drug Discovery and Development Settings. *Advanced Drug Delivery Reviews*, 46(1-3), 3–26. doi: 10.1016/S0169-409X(00)00129-0
- Liu, X., Zhang, B., Jin, Z., Yang, H., & Rao Z. (2020). 7BQY The Crystal Structure of Covid-19 Main Protease in Complex With An Inhibitor N3 at 1.7 Angstrom. Retrieved from <https://www.rcsb.org/structure/7BQY>. doi: 10.2210/pdb7BQY/pdb
- Lovell, S. C., Davis, I. W., Adrendall, W. B., de Bakker, P. I. W., Word, J. M., Prisant, M. G., Richardson, J. S., & Richardson, D. C. (2003) Structure Validation by C $\alpha$  Geometry:  $\phi$ ,  $\psi$  and C $\beta$  Deviation. *Proteins: Structure, Function, and Bioinformatics*, 50(3), 437–450. doi: 10.1002/prot.10286
- Lu, H.-M., Yin, D.-C., Ye, Y.-J., Luo, H.-M., Geng, L.-Q., Li, H.-S., Guo, W.-H., & Shang, P. (2009). Correlation Between Protein Sequence Similarity and X-Ray Diffraction Quality in The Protein Data Bank. *Protein & Peptide Letters* 16, 50–55. doi: 10.2174/092986609787049457
- Meng, X.-Y., Zhang, H.-X., Mezei, M., & Cui, M. (2012). Molecular Docking: A Powerful Approach for Structure-Based Drug Discovery. *Current Computer Aided-Drug Design*, 7(2), 146–157. doi: 10.2174/157340911795677602
- MolProbity. (2020). Analysis output: geometry for 7bqy.pdb. Retrieved from <http://molprobity.biochem.duke.edu/index.php?MolProbSID=k7t41ngp2o2kmb4tpfi4d0amf0&eventID=62> [October, 29th, 2020]
- Morris, G.M., Huey, R., Lindstrom, W., Sanner, M.F., Belew, R. K., Goodsell, D.S., & Olson, A.J. (2009). Autodock4 and AutoDockTools4: automated docking with selective receptor flexibility. *Journal of Computational Chemistry*, 16, 2785-2791
- Narkhede, R. R., Cheke, R. S., Ambhore, J. P., shinde, S.D. (2020). the molecular docking study of potential drug candidates showing anti-COVID-19 activity by exploring of therapeutic targets of SARS-CoV-2. *Eurasian Journal of Medicine and Oncology*, 4(3), 185-195. doi: 0.14744/ejmo.2020.31503
- O'Boyle, N.M., Banck, M., James, C.A., Morley, C., Vandermeersch, T., & Hutchison, G.R. (2011).

- Open Babel: An Open Chemical Toolbox. *Journal of Cheminformatics*, 3, 33. doi:10.1186/1758-2946-3-33
- Open Babel. The Open Babel Package, version 2.3.1. Retrieved from <http://openbabel.org> (accessed May 2020)
- Pasetto, S., Pardi, V., & Murata, R.M. (2014). Anti-HIV-1 Activity of Flavonoid Myricetin on HIV-1 Infection in a Dual-Chamber In Vitro Model. *PLoS ONE*, 9(12), 1–18. doi: 10.1371/journal.pone.0115323
- Prajapat, M., Sarma, P., Shekhar, N., Avti, P., Sinha, S., Kaur, H., Kumar, S., Bansal, S., & Medhi, B. (2020). Drug Targets for Corona Virus: A Systematic Review. *Indian Journal of Pharmacology*, 52(1), 56-65. doi: 10.4103/ijp.IJP\_115\_20
- Prisant, M. G., Williams, C. J., Chen, V. B., Richardson, J. S., & Richardson, D. C. (2020). New tools in MolProbity validation: CaBLAM for CryoEM backbone, UnDowser to rethink “waters,” and NGL Viewer to recapture online 3D graphics. *Protein Science*, 29, 315-329. doi: 10.1002/pro.3786
- Salim, B. & Noureddine, M. (2020). Identification of compounds from *Nigella sativa* as new potential inhibitors of 2019 novel coronavirus (Covid-19): molecular docking study. *ChemRxiv*, Preprint. doi: 10.26434/chemrxiv.12055716.v1
- Schleinkofer, K., Wang, T., & Wade, R.C. (2006). Molecular Docking. *Encyclopedic Reference of Genomics and Proteomics in Molecular Medicine*, 443, 1149–1153. doi: 10.1007/3-540-29623-9\_3820
- Shibata, C., Ohno, M., Otsuka, M., Kishikawa, T., Goto, K., Muroyama, R., Kato, N., Yoshikawa, T., Takata, A., & Koike, K. (2014). The Flavonoid Apigenin Inhibits Hepatitis C virus replication by Decreasing Mature MicroRNA122 Levels. *Virology*, 462-463(1), 42–48. doi: 10.1016/j.virol.2014.05.024
- Sithisarn, P., Michaelis, M., Schubert-Zsilavecz, M., & Cinatl, J. (2013). Differential antiviral and Anti-Inflammatory Mechanisms of The Flavonoids Biochanin A and Baicalein in H5N1 Influenza A Virus-Infected Cells. *Antiviral Research*, 97(1), 41–48. doi: 10.1016/j.antiviral.2012.10.004
- Sun, J., He, W.-T., Wang, L., Lai, A., Ji, X., Zhai, X., Li, G., Suchard, M. A., Tian, J., Zhou, J., Veit, M., & Su, S. (2020). COVID-19: Epidemiology, Evolution, and Cross-Disciplinary Perspectives. *Trends in Molecular Medicine*, 26(5), 483-495. doi: 10.1016/j.molmed.2020.02.008
- Takahashi, H., Iwasaki, Y., Watanabe, T., Ichinose, N., Okada, Y., Oiwa, O., Kobayashi, T., Moriya, M., Oda, T. (2020). Case studies of SARS-CoV-2 treated with favipiravir among patients in critical or severe condition. *International Journal of Infectious Diseases*, 100, 283-285. doi: 10.1016/j.ijid.2020.08.047
- Tobergte, D. R., & Curtis, S. (2015). Anti-Inflammatory, Antipyretic, and Analgesic Agents. *Lippincott Illustrated Reviews Pharmacology*, 53(9), 1689–1699. doi: 10.1017/CBO9781107415324.004
- Trott, O., & Olson, A.J. (2010). Autodock Vina: improving the speed and accuracy of docking with a new scoring function, efficient optimization and multithreading. *Journal of Computational Chemistry*, 31, 455-461
- Ullrich, S., & Nitsche, C. (2020). The SARS-CoV-2 Main Protease as Drug Target. *Bioorganic & Medicinal Chemistry Letters*, 30(17), 127377. doi: 10.1016/j.bmcl.2020.127377
- Wallace, A. C., Laskowski, R. A., Thornton J. M. (1995). LIGPLOT: A program to generate schematic diagrams of protein-ligand interactions. *Protein Engineering*, 8, 127-134
- Wu, C., Liu, Y., Yang, Y., Zhang, P., Zhong, W., Wang, Y., Wang, Q., Xu, Y., Li, M., Li, X., Zheng, M., Chen, L., & Li, H. (2020). Analysis of Therapeutic Targets for SARS-CoV-2 and Discovery of Potential Drugs by Computational Methods. *Acta Pharmaceutica Sinica B*, 10(5), 766-788. doi: 10.1016/j.apsb.2020.02.008
- Zhang, W., Qiao, H., Lv, Y., Wang, J., Chen, X., Hou, Y., Tan, R., & Li, E. (2014). Apigenin Inhibits Enterovirus-71 Infection by Disrupting Viral RNA Association with Trans-Acting Factors. *PLoS ONE*, 9(10), 1–9. doi: 10.1371/journal.pone.0110429
- Zhu, N., Zhang, D., Wang, W., Li, X., Yang, B., Song, J., Zhao, X., Huang, B., Shi, W., Lu, R., Niu, P., Zhan, F., Ma, X., Wang, D., Xu, W., Wu, G., Gao, G. F., & Tan, W. (2020). A Novel Coronavirus from Patients with Pneumonia in China, 2019. *The New England Journal of Medicine*, 382(8), 727–733. doi: 10.1056/NEJMoa2001017